Applied Surface Science 270 (2013) 16–24

Contents lists available at SciVerse ScienceDirect

Applied Surface Science

journal homepage: www.elsevier.com/locate/apsusc

Chemical evolution of InP/InGaAs/InGaAsP microstructures irradiated in air and deionized water with ArF and KrF lasers

Neng Liu, Jan J. Dubowski*

Laboratory for Quantum Semiconductors and Photon-based BioNanotechnology, Interdisciplinary Institute for Technological Innovation (3IT), Department of Electrical and Computer Engineering, Université de Sherbrooke, Québec, J1K 2R1, Canada

ARTICLE INFO

Article history:
Received 7 October 2012
Accepted 1 December 2012
Available online 4 January 2013

Keywords:
Quantum well intermixing
InP/InGaAs/InGaAsP microstructures
ArF and KrF excimer laser irradiation
X-ray photoelectron spectroscopy
Secondary ion mass spectroscopy
Indium and InP oxides

ABSTRACT

Irradiation of quantum semiconductor microstructures with ultraviolet pulsed lasers could induce surface defects and modify chemical composition of the microstructure capping material that during high-temperature annealing leads to selected area bandgap engineering through the process known as quantum well intermixing (QWI). In this work, we investigate the role of both ArF and KrF excimer lasers in the QWI process of InP/InGaAs/InGaAsP microstructures irradiated in air and deionized (DI) water. X-ray photoelectron spectroscopy and secondary ion mass spectroscopy analysis was employed to study the chemical composition of the irradiated surface and investigate the chemical evolution of ArF and KrF laser irradiated microstructures. The results indicate that InP_xO_y oxides are the dominating surface products of the ArF and KrF lasers interaction with InP. Consistent with this observation is a relatively greater bandgap blue shift of ~130 nm found in the microstructures irradiated in air, in comparison to a maximum of 60 nm blue shift observed in the microstructures irradiated in a DI water environment.

1. Introduction

Quantum well intermixing (QWI) has been reported as a potentially efficient method for the fabrication of some photonic integrated circuits due to its ability to selective area modify the bandgap of quantum well (QW) or quantum dot microstructures [1–3]. InP/InGaAs/InGaAsP QW microstructures, due to their ability to address device fabrication for fiber optic communication at 1.3 and 1.55 μm wavelengths, i.e., where the optical fibers exhibit the minimum of optical attenuation, have attracted a significant volume of QWI investigations [4–6]. In addition to traditionally investigated QWI techniques, excimer lasers were found attractive as they are able to induce surface defects and modify chemical composition of the microstructures capping material that during rapid thermal annealing (RTA) could lead to QWI-based selective area bandgap engineering [7–10]. Depending on whether a QW microstructure is irradiated directly in air [8,11] or through a dielectric cap layer [12,13] different bandgap shifts have been observed, indicating the importance of the environment on the nature of surface defects and their role in the QWI mechanism. The role of surface defects, including P vacancies and In interstitials created in the InP cap layer irradiated with Ar ions, has been investigated with X-ray photoelectron spectroscopy (XPS) [14] and revealed that, indeed, the modification of the surface chemical composition plays an important role in the QWI process. The XPS and Auger spectroscopy techniques have also been employed to study surface chemistry of excimer laser irradiated InP [8] and InGaAs/InGaAsP microstructures [15], indicating that the amount of surface oxides normally increases with the laser pulse number if the irradiation is carried out in an air atmosphere. Although the influence of the presence of different oxides, such as SiO_2, SiO_xN_y and TiO_x deposited on quantum semiconductor (QS) microstructures on the QWI effect has been reported in literatures [3,16,17], the correlation between the amplitude of the QWI effect (bandgap shifting) and the concentration of specific oxides induced with lasers has remained a relatively weakly investigated problem.

The presence of various atomic species in QW microstructures at the impurity level of $<10^{19}$ cm^{-3} is known to contribute to the QWI effect [18,19]; therefore the investigation of excimer laser induced QWI effect has to address the problem of impurities distribution in irradiated microstructures. With this in mind, we have employed the time of flight secondary ion mass spectroscopy (TOF-SIMS) due to its high sensitivity and possibility of providing depth profiles of impurities in multilayer microstructures [20,21]. Of particular interest was the influence of the irradiation environments of air

* Corresponding author. Tel.: +1 819 821 8000; fax: +1 819 821 7937.
E-mail address: jan.j.dubowski@usherbrooke.ca (J.J. Dubowski).
URL: http://www.dubowski.ca (J.J. Dubowski).

0169-4332/$ – see front matter © 2012 Elsevier B.V. All rights reserved.
http://dx.doi.org/10.1016/j.apsusc.2012.12.007

and deionized (DI) water on the amplitude of bandgap shifting and the quality of the intermixed material.

2. Experiment details

The investigated InP/InGaAs/InGaAsP microstructure consists of five (5) 6-nm-thick $In_{0.47}Ga_{0.53}As$ wells separated by four (4) 10-nm-thick $In_{0.74}Ga_{0.26}As_{0.57}P_{0.43}$ barriers. It comprises 110 and 20 nm thick InGaAsP graded bandgap layers, interfacing the substrate and surface side of the QW stack, that have been designed to provide optical waveguiding confinement. The microstructure is covered with a 40-nm thick InP and a 6-nm-thick etch-stop InGaAsP layer and, finally, capped with a 30-nm thick InP layer. The microstructure was designed to emit photoluminescence (PL) at 1.540 μm at room temperature. Small samples, typically 10 mm × 10 mm, were cleaved from the QW wafer and degreased in opticlear, acetone and isopropyl alcohol, each for 5 min at room temperature. For the laser irradiation experiments, the samples were installed in a 0.74 mm high chamber made of UV transparent (T > 90%) fused silica glass. The sample chamber was filled either with air or DI water. The irradiation was carried out with ArF (λ = 193 nm) and KrF (λ = 248 nm) excimer lasers (Lumonics, Pulse Master 800). The laser beam, homogenized with a double microlens fly-eye-array, was used to irradiate a circular mask. The image of the mask was projected on the sample surface at demagnification ratios of 2.6 and 1.8 with the ArF and KrF laser setups, respectively. A computer controlled X–Y–Z-Theta sample holding stage allowed for processing of the same sample at numerous sites. Following the laser irradiation, the samples were installed in a sealed nitrogen container to limit their exposure to an atmospheric environment, and transported for further processing. After laser irradiation, the samples were annealed for 2 min at 700 °C with a rapid thermal annealing (RTA) furnace (JIPELEC, Jetfirst) in an atmosphere of mixed hydrogen and nitrogen forming gas (N_2:H_2 = 1:9).

Room temperature PL measurements of investigated samples were carried out with a commercial mapper (Philips, PLM-150) that employs an Nd:YAG laser (λ = 1.06 μm) to excite the samples. The PL signal was collected with a spatial resolution of 30 μm, dispersed by a monochromator and detected by an InGaAs photodiode array.

The XPS measurements were carried out in a spectrometer (Kratos Analytical, AXIS Ultra DLD) equipped with a 150 W Al Kα source and operating at a base pressure of 1×10^{-9} Torr. The surface survey scan and high resolution scans were observed in constant energy modes at 50 eV and 20 eV pass energy, respectively. The size of an analyzed area on the investigated samples was set at 220 μm × 220 μm. The XPS spectra were recorded for samples after laser irradiation and after the RTA step. The collected data were processed using Casa XPS 2.3.15 software. To compensate for the surface charging effect, all XPS data binding energies were referenced to the adventitious C (C_{adv}) 1s peak at the binding energy (BE) of 285.0 eV. For spectral fitting, Gaussian-type and asymmetric peaks with constant full width at half-maximum (FWHM) were used for all components at a particular peak envelope. Quantification of XPS data was obtained by determining the area under each component peak that was corrected using manufacturer's relative sensitivity factors (RSF). The RSF used for In 3d, P 2p and O 1s were set at 13.3, 1.19 and 2.93, respectively.

TOF-SIMS (TOF-SIMS IV, ION-TOF GmbH) measurements were performed to record information about the chemical composition and obtain depth profiles of atoms in non-irradiated sites, and sites irradiated in air and DI water before and after RTA. A 10 keV Bi ion beam was used as an analysis gun and a 3 keV Cs ion source was used as a sputtering gun. The sputtering beam was rastered over an area of 500 μm × 500 μm in the center of irradiated spots and the analysis signal was taken from a 50 μm × 50 μm area in the center of the sputtered region.

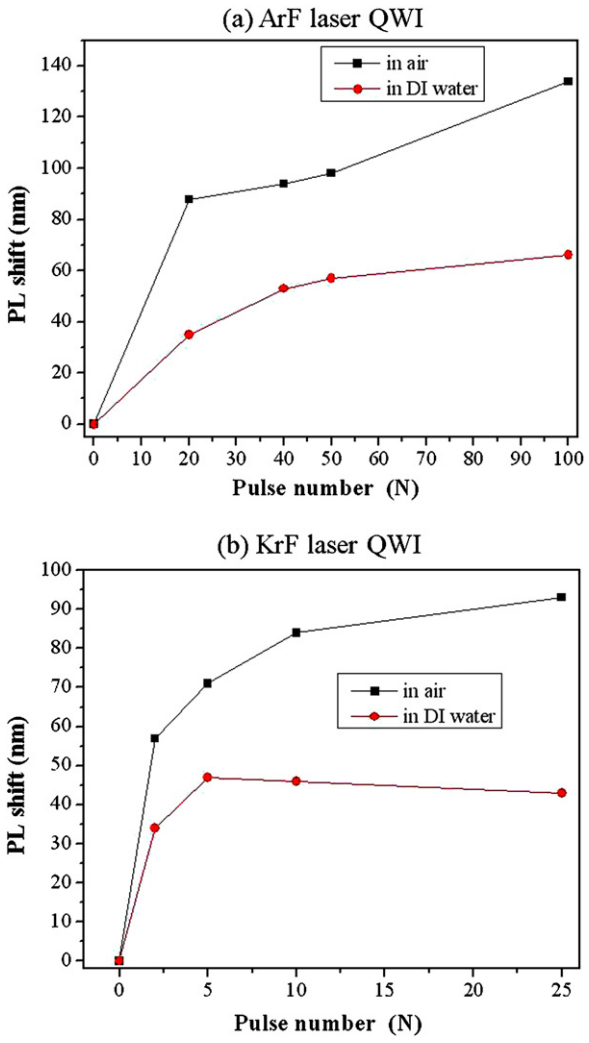

Fig. 1. PL shift dependence in the InP/InGaAs/InGaAsP microstructure on the laser pulse number after (a) ArF and (b) KrF laser irradiation in air and DI water that was followed by the RTA step.

3. Results and discussions

3.1. PL in InP/InGaAs/InGaAsP microstructure irradiated in air and DI water

Fig. 1 illustrates the PL shift dependence on pulse number in InP/InGaAs/InGaAsP microstructure after ArF laser irradiation at 82 mJ/cm^2 (Fig. 1a) and KrF laser irradiation at 124 mJ/cm^2 (Fig. 1b) in air and DI water and RTA at 700 °C for 2 min. For samples irradiated in air by both lasers, the PL shift continues to increase with the pulse number and it saturates for $N \geq 25$ pulses for KrF irradiated samples, while no such saturation is visible for the ArF irradiated samples, even for N = 100 pulses. The maximum blue shift of 130 nm observed for the ArF irradiated samples compares to 90 nm of the maximum blue shift observed for the KrF irradiated samples. In contrast, for samples irradiated in DI water, the saturation of the blue shift amplitude is observed at $N \geq 20$ and $N \approx 5$ for ArF and KrF irradiated samples, respectively. The blue shift saturation amplitude of near 60 nm seems to be related to the limited concentration of the intermixing inducing defects that both lasers can generate during the irradiation in a DI water environment.

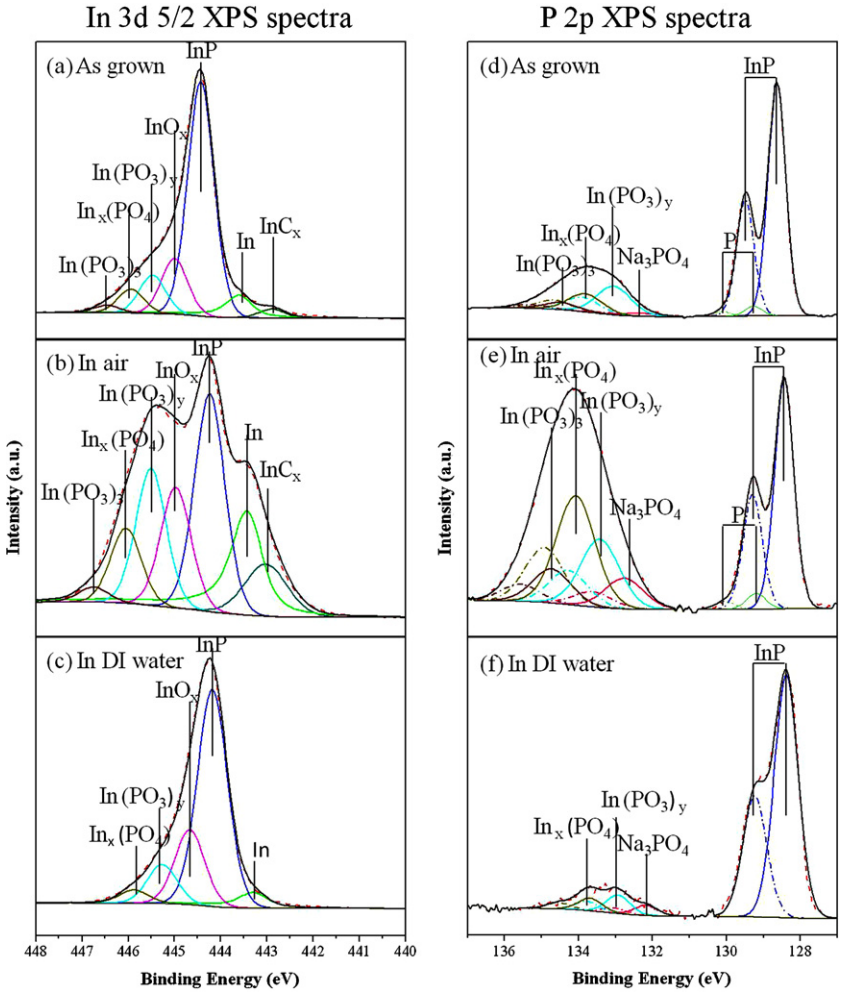

Fig. 2. In 3d 5/2 and P 2p XPS spectra of as grown sample (a and d), and a sample irradiated by ArF laser at 82 mJ/cm^2 with 50 pulses in air (b and e) and in DI water (c and f).

A slightly stronger absorption of InP at 4.99 eV ($\sim 1.77 \times 10^6$ cm^{-1}) than at 6.4 eV ($\sim 1.25 \times 10^6$ cm^{-1}) [22] could result in a modification of the thicker surface layer achieved with the ArF laser and, as a result, lead to a greater QWI amplitude as illustrated in Fig. 1a. Note that even though the microstructure was irradiated with 50% more intense pulses of the KrF laser in comparison to those of the ArF laser (124 vs 82 mJ/cm^2), the energy absorbed by the samples was comparable in both cases due to a greater reflectivity of InP at 4.99 eV ($R \sim 0.6$) than at 6.4 eV ($R \sim 0.43$) [22]. Nevertheless, the role of the irradiation environment is clear, as the maximum blue shift amplitudes achieved with both lasers are significantly smaller for samples irradiated in DI water than for samples irradiated in air.

3.2. XPS analysis of sample irradiated by ArF laser in air and in DI water

Fig. 2 shows In 3d 5/2 and P 2p XPS spectra of cap InP surface for as grown (non-irradiated) sample (a, d), irradiated by ArF laser in air (b, e) and DI water (c, f) with 50 pulses at 82 mJ/cm^2. The In 3d 5/2 spectra from all the samples have been fitted with elemental In (BE = 443.5 ± 0.2 eV, FWHM = 0.67 eV), InP (BE = 444.4 ± 0.2 eV, FWHM = 0.67 eV), indium oxide (InO_x) (BE = 445.2 ± 0.2 eV, FWHM = 0.67 eV) and $In(PO_3)_y$ (BE = 445.6 ± 0.2 eV, FWHM = 0.67 eV), $In_x(PO_4)$ (BE = 446.3 ± 0.2 eV, FWHM = 0.67 eV) [23–25]. All the peaks have been fitted with Gaussian functions, except for In, where an asymmetric function has been used [26]. A peak at the highest binding energy (BE = 446.4 ± 0.2 eV, FWHM = 0.67 eV) observed for the as-grown and air irradiated samples, has been attributed to $In(PO_3)_3$. This peak disappeared in the spectra of samples irradiated in DI water, consistent with the high solubility of InP_xO_y oxides in water [27]. Also, for these two samples, as illustrated in Fig. 2 a and b, an additional peak has been observed at the lowest binding energy (443.0 ± 0.2 eV). As this peak appears accompanied with the appearance of the carbide peak in C 1s spectrum, we ascribed it to indium carbide, InC_x [28,29]. This peak is absent in the sample irradiated in DI water, as shown in Fig. 2 c.

A comparison between Fig. 2 a, b and c shows that the concentration of InO_x and InP_xO_y has significantly increased in the air-irradiated sample, and additional oxides, such as $In(PO_3)_y$, $In_x(PO_4)$ and $In(PO_3)_3$, have also been created by the ArF laser irradiation in air. Using a model reported in the literature [30], our COMSOL calculations indicated that the peak temperature of InP irradiated with the ArF laser at 82 mJ/cm^2 in air is about 500 K. This condition leads to the formation of InO_x and InP_xO_y by adsorption of oxygen that enters the In—In and In—P bonds [31]. In contrast, the irradiation in DI water with the same laser fluence induces a peak temperature of about 360 K. At this temperature, no significant oxidation of InP is expected. Besides, laser heated DI water environments will enhance desorption of phosphorous oxides by the dissolution process [27]. The oxygen concentration in DI water is lower than that in air [32], which is consistent with the low XPS intensity of InO_x and InP_xO_y components observed in Fig. 2 c. We

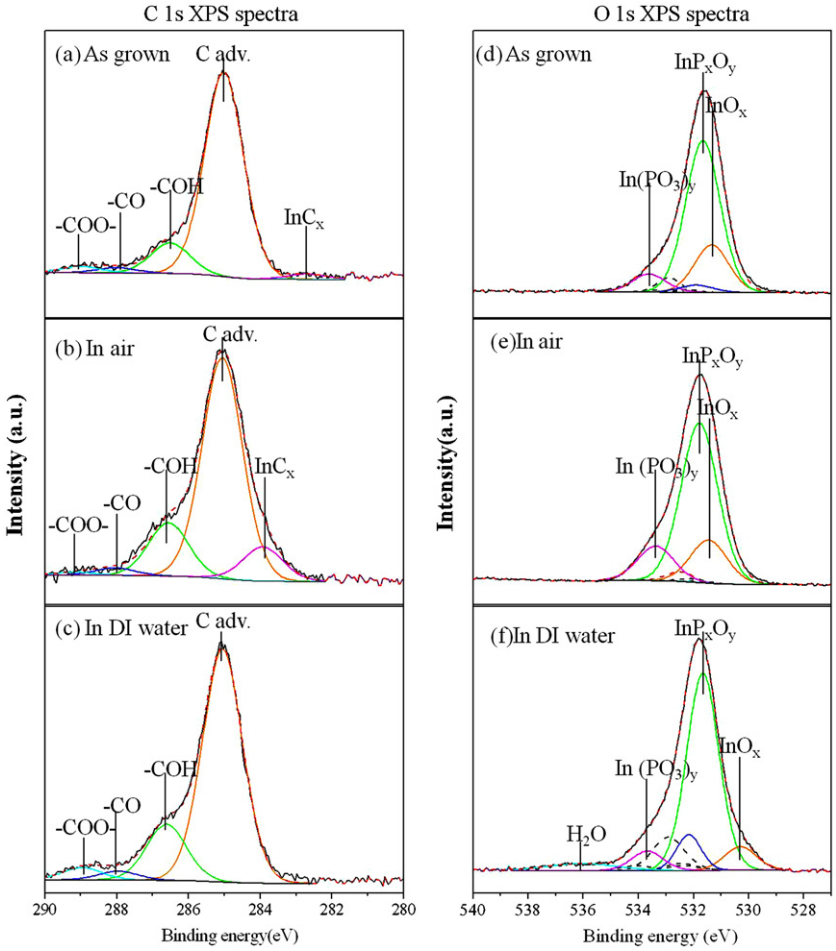

Fig. 3. C 1s and O 1s XPS spectra of as grown sample (a and d) and a sample irradiated by ArF laser at 82 mJ/cm^2 with 50 pulses in air (b and e) and in DI water (c and f).

note that the binding energy of InO_x created in DI water has been reduced by 0.3 eV and the In/O ratio has decreased from 1.3 in air to 0.8 in DI water. This suggests that another In sub-oxides are created in the sample irradiated in DI water [33].

The P 2p spectra in Fig. 2d, e and f show 2p 3/2 (solid line) and 2p 1/2 (dash dot line) doublets of InP and P, respectively. To fit the experimental data, we fixed the doublet separation and branch ratio of P 2p 3/2 to P 2p 1/2 at 0.85 eV and 2.0, respectively. The peaks at low binding energy (BE = 128.6 ± 0.2 eV, FWHM = 0.56 ± 0.1 eV) were assigned to InP and the peaks at secondary higher binding energy (BE = 129.2 ± 0.1 eV, FWHM = 0.56 ± 0.1 eV) were assigned to P [34]. The oxides at the higher binding energy can be ascribed to $In(PO_3)_y$ (BE = 133.1 ± 0.2 eV, FWHM = 1.1 ± 0.1 eV), $In_x(PO_4)$ (BE = 133.8 ± 0.2 eV, FWHM = 1.1 ± 0.1 eV) and $In(PO_3)_3$ (BE = 134.4 ± 0.2 eV, FWHM = 1.1 ± 0.1 eV), consistent with those in the In 3d 5/2 spectra[35]. For the sample irradiated in air (Figure 2e), the XPS intensity of InP_xO_y increased significantly. However, for the sample irradiated in DI water (Figure 2f), the quantity of InP_xO_y has reduced and $In(PO_3)_3$ has clearly disappeared due to dissolution. The P 2p XPS spectra are consistent with the In 3d 5/2 XPS spectra.

Fig. 3 shows the C 1s and O 1s XPS spectra of as-grown sample (a, d) and sample irradiated by ArF laser at 82 mJ/cm^2 with 50 pulses in air (b, e) and DI water (c, f). The C 1s XPS spectra are dominated by the C_{adv} peak that was assigned to 285.0 eV and used for the calibration of the charging effect. All the C 1s spectra showed the presence of three additional C adsorbate species: alcohol —COH (286.5 ± 0.2 eV), carbonyl —CO (287.9 ± 0.1 eV) and ester —COO— (288.8 ± 0.1 eV) [36]. The peak at lower binding energy (≤284 eV) in the C 1s XPS spectra of the as-grown and air irradiated samples could be assigned to metal carbide [37]. Here, we attributed it to InC_x, which is consistent with the results shown by the In 3d 5/2 spectra (see Fig. 2a, b) that also show the increased quantity of this carbide in the sample irradiated in air. The binding energy of the InC_x peak observed for the laser-irradiated sample (Fig. 3b) has been increased by 0.5 eV, in agreement with the reported high-temperature reconstruction of this compound [38]. However, the InC_x peak disappeared in the sample irradiated in DI water, similarly to what has been observed in the In 3d 5/2 spectra.

Four small peaks corresponding to the O-containing C adsorbates have been observed in the O 1s spectra in Fig. 3d, e and f. The intensities of these peaks are related to the corresponding species in C 1s spectrum in Fig. 3a, b and c. Identification of these C adsorbates species in the O 1s peak is important for the analysis of the quantities of InO_x and InP_xO_y. The expanded portion of the O 1s peak at higher binding energy of the as grown and irradiated in air and DI water samples are shown Fig. 4a, b and c. In addition to the C adsorbate peaks, the peak at 532.0 ± 0.2 eV has been ascribed to absorbed oxygen species (see Fig. 4) and the other peak at 533.7 ± 0.2 eV has been ascribed to bridging oxygen atoms in $In(PO_3)_y$ (see Fig. 3) [35]. The expanded view of the O1s spectrum (Fig. 4c) of the sample irradiated in DI water shows the presence of the H_2O peak at BE = 536.0 ± 0.2 eV. A similar peak has been reported for a rhenium sample irradiated in DI water [39]. Note that the binding energy of InO_x created in DI water (Fig. 3f) has been reduced by ~1.2 eV and the In/O ratio has decreased from 1.3 to 0.8 in DI water, which means another kind of indium oxides created [40]. This is consistent with the formation of a low binding energy non-stoichiometric

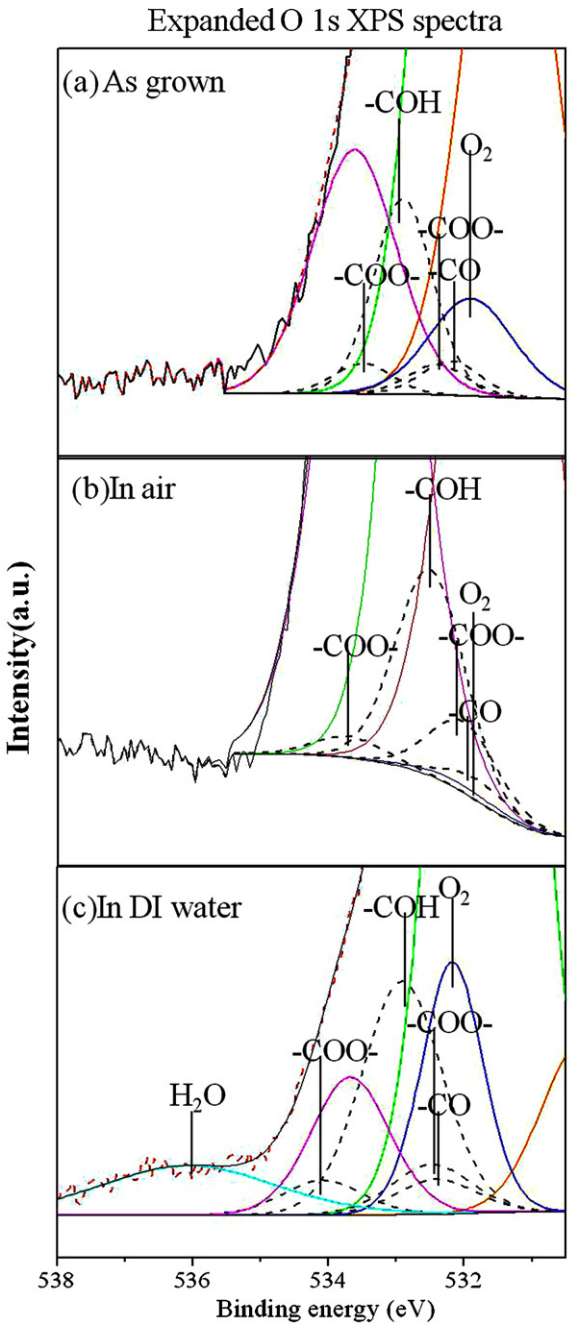

Fig. 4. Expanded O 1s XPS spectra of the as grown sample (a) and the sample irradiated by ArF laser at 82 mJ/cm^2 with 50 pulses in air (b) and in DI water (c).

sub-oxide compound that is energetically stable, even at temperature approaching 1000 °C [33].

3.3. XPS analysis of sample irradiated by ArF laser in air and DI water and then RTA

The In 3d 5/2 and P 2p XPS spectra of RTA as-grown samples and RTA ArF laser irradiated samples at 82 mJ/cm^2 with 50 pulses in air and DI water are shown in Fig. 5. Compared with Fig. 2, these spectra demonstrate that the RTA step has drastically reduced the concentration of surface oxides in all samples. This reduction is primarily related to the decomposition process of P-oxides as it is known that P atoms evaporate at 650 °C [41] and InP_xO_y decomposes at 458 °C [42]. Some presence of InC_x can be seen in the air irradiated samples (Fig. 5b), but the carbide disappeared in the RTA as-grown sample (Fig. 5a) and in the RTA sample laser-irradiated in DI water (Fig. 5c). It is possible that surface oxides and carbides could be the source of O and/or C diffusing into the QW region, which would promote the QWI process. However, the role of C in the intermixing process seems negligible due to a relatively small concentration of this impurity at the surface of laser-irradiated samples, especially those processed in the DI water environment. Furthermore, the diffusion coefficient of C in GaAs is relatively low ($<10^{-16}$ cm^2 s^{-1}) [43] in comparison to the defect diffusion rate of 2.3×10^{-15} cm^{-2} s^{-1} reported for a similar InGaAs QW structure during pulsed Nd:YAG laser QWI [44].

Fig. 6 shows the C 1s and O 1s XPS spectra of the as-grown sample (Fig. 6a and d) and the sample irradiated with the ArF laser in air (Fig. 6b and e) and DI water (Fig. 6c and f) with 50 pulses at 82 mJ/cm^2 and then RTA at 700 °C for 2 min. It can be seen that the trace of H_2O, previously observed for a sample irradiated in DI water (see Fig. 3f) has disappeared following the high temperature treatment. The intensity of the InO_x peak observed in the O 1s spectra has also decreased considerably, especially in the as-grown sample and that irradiated with the laser in air. However, the InO_x peaks in the as-grown sample and irradiated in air has shifted to low binding energy (530.0 ± 0.2 eV), which is similar as that in the sample irradiated in DI water, consistent with the more stable form of In sub-oxide after high temperature treatment [33]. The InC_x feature in the C 1s spectrum of the sample irradiated in air is practically invisible.

Fig. 7 presents a dependence of the XPS atomic concentrations of In, InP, oxides compounds and major adsorbates observed at the surface of the InP capping layer as a function of the laser irradiation pulses. The results are presented for samples irradiated in DI water (Fig. 7a and c) and air (Fig. 7b and d) using 82 mJ/cm^2 pulses of the ArF laser. It can be seen that the InP_xO_y XPS signal from the sample irradiated in air increases rapidly with the number of laser pulses to reach a plateau at $N \geq 40$. This increase is mirrored by a decrease of the InP XPS signal observed for the same range of laser pulses. In contrast, the concentration of InP_xO_y in the sample irradiated in DI water increases weakly (about 5%) for $0 < N \leq 50$. At the same time, the O_2 XPS signal remains relatively unchanged, or even slightly reduced for $0 < N \leq 40$ in comparison to that in the sample irradiated in air (compare Fig. 7a and b). Similarly, the InO_x concentration increased by 6% in the sample irradiated in air while the quantity of this compound in the sample irradiated in DI water doesn't show an obvious increase. Thus, the weaker formation of oxides on the surface of samples processed in DI water, as well as water dissolution of oxides appear the main reason for the pulse dependent behavior of the InP XPS signal observed in Fig. 7a.

Following the RTA treatment at 700 °C for 2 min, both series of samples show comparable XPS composition profiles for the range of $0 \leq N \leq 100$. It is feasible that the surface oxides have been decomposed and/or evaporated during the RTA step, although some diffusion of the surface adsorbates could take place into the investigated microstructures.

3.4. SIMS analysis of RTA samples that were irradiated with ArF laser in air and DI water

The TOF-SIMS depth profiles of oxygen in the QW microstructures irradiated with the ArF laser are shown in Fig. 8. The bars above the figures illustrate the chemical composition of the investigated microstructure. The five InGaAs wells and four InGaAsP barriers separating the wells can clearly be identified from the observed oxygen profiles. The presence of oxygen is a common problem in CBE [45] and MOVPE [46] grown materials. The concentration of oxygen in the InGaAs layers reported in Fig. 8a is lower than in the InGaAsP layers, consistent with the use of PH_3 for the

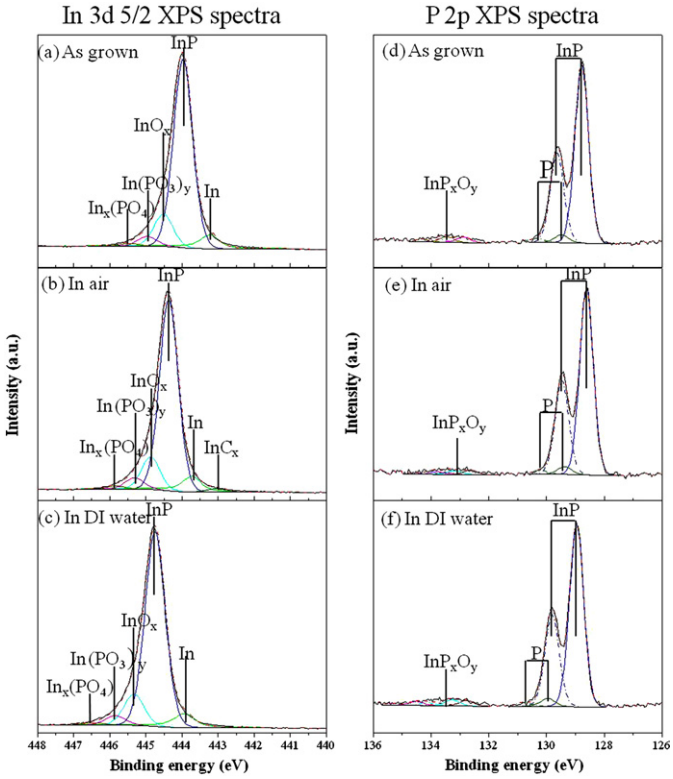

Fig. 5. In 3d 5/2 and P 2p XPS spectra of as grown sample (a and d) and a sample irradiated by ArF laser at 82 mJ/cm^2 with 50 pulses in air (b and e) and DI water (c and f), followed by the RTA step.

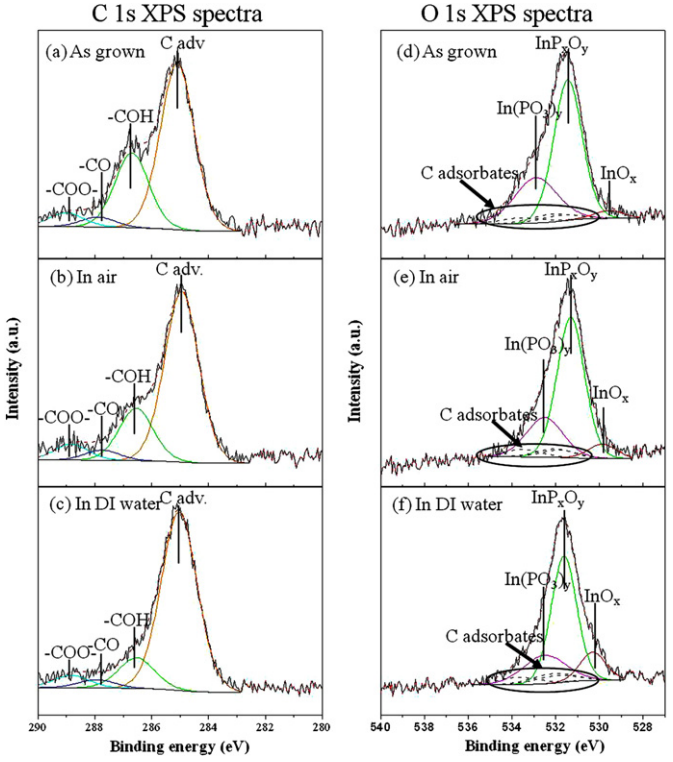

Fig. 6. C 1s and O 1s XPS spectra of as grown sample (a and d) and a sample irradiated by ArF laser at 82 mJ/cm^2 with 50 pulses in air (b and e) and DI water (c and f), followed by the RTA step.

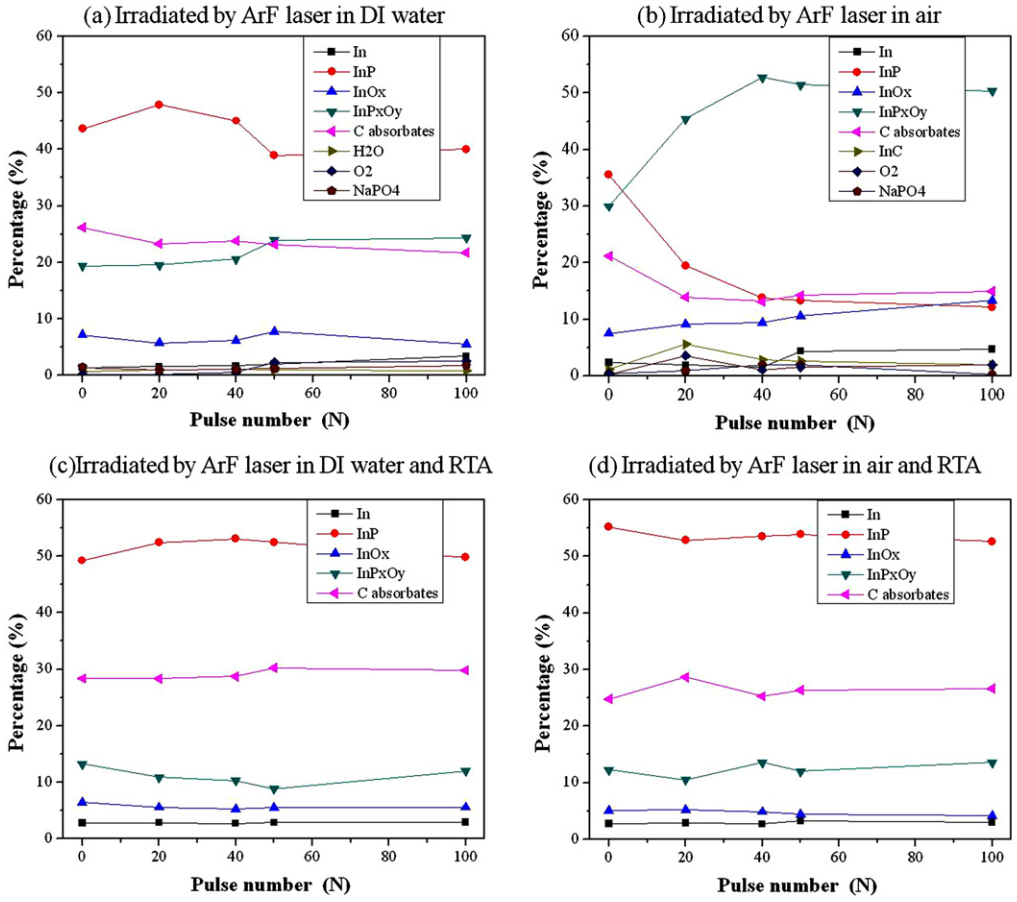

Fig. 7. Dependence of XPS atomic concentration of InP and surface adsorbates on the laser pulse number in samples irradiated with ArF laser in DI water (a), in air (b) and after RTA of the sample irradiated in DI water (c) and in air (d).

growth of the barrier material that could also be the source of the oxygen impurity. The SIMS oxygen profiles for the as-grown and irradiated in DI water samples are almost identical. However, the laser irradiation in air has induced a measurable increase of oxygen in the top portion of the microstructure (sputtering time < 600 s). For the same sample, the diffusion of oxygen into the entire active region of the microstructure has been observed following the RTA step at 700 °C for 2 min (Fig. 8b). For the sample irradiated in DI

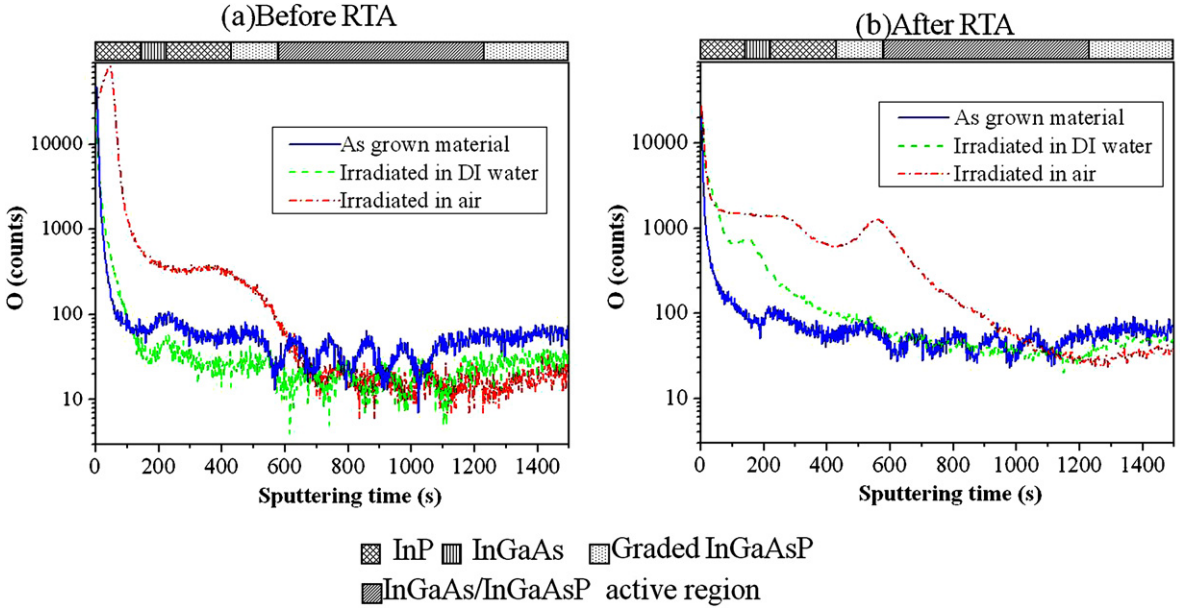

Fig. 8. TOF-SIMS oxygen concentration depth profile in as grown sample, and in samples irradiated with ArF laser in DI water and in air before (a) and after (b) RTA at 700 °C for 2 min.

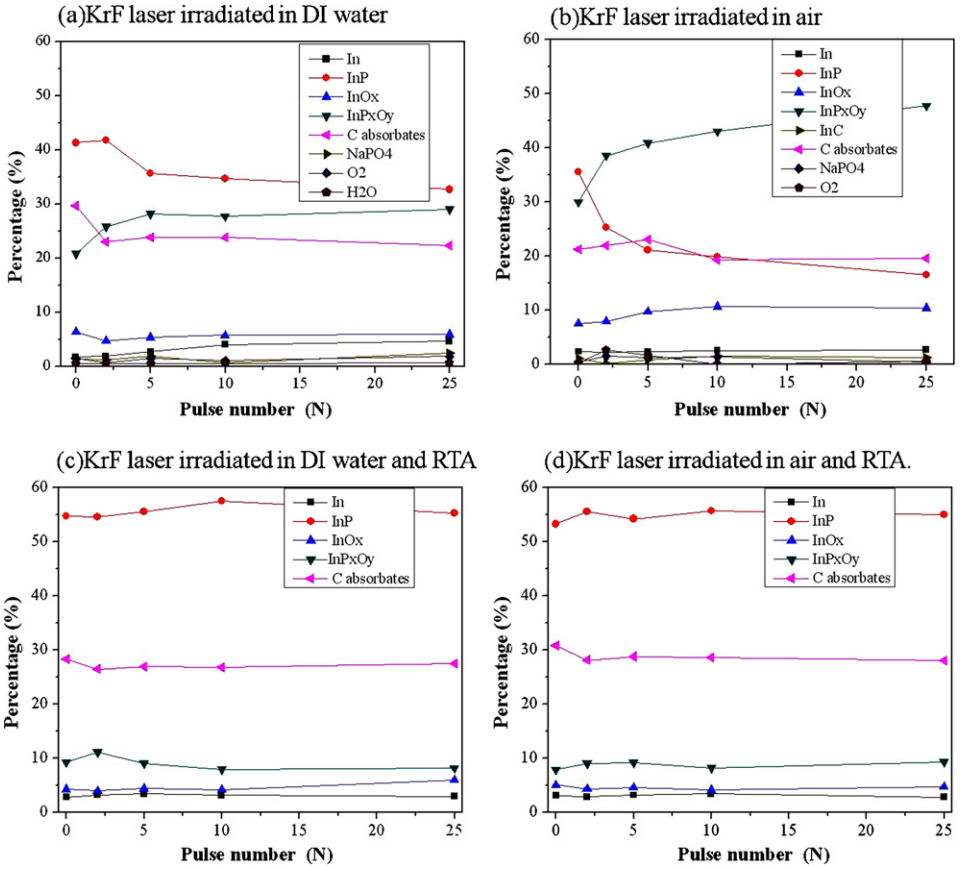

Fig. 9. Dependence of XPS atomic concentration of InP and surface adsorbates on the laser pulse number in the sample irradiated with KrF laser in DI water (a), in air (b) and after RTA of the sample irradiated in DI water (c) and in air (d).

water, the RTA step increased the oxygen concentration only in the top portion of the microstructure (sputtering time < 500 s).

The oxygen impurity in III–V QW microstructures has been employed to enhance intermixing in a sample coated with Al-reduced SiO_2 intermixing [47]. It seems reasonable that this impurity is the main source of the QWI effect observed in the investigated here microstructures.

3.5. XPS analysis of the samples after KrF laser irradiation in air and in DI water

Qualitatively, similar results have been observed for the KrF laser irradiated samples. Fig. 9 presents XPS atomic concentrations of In, InP, oxides compounds and major adsorbates observed for the as-grown InP cap layer and a dependence of these concentrations on the laser irradiation pulse number. The irradiation was carried out in DI water and air environments using the KrF laser delivering pulse fluence of 124 mJ/cm^2. For the samples irradiated in DI water, a 25-pulse irradiation increases atomic concentration of InP_xO_y to 28%, while the same irradiation in air results in the increase of the concentration of this oxide to 48%. The XPS InP signal decreases with the pulse number as it has been oxidized into InP_xO_y. This effect is especially evident for samples irradiated in air. For the samples irradiated in air, the concentration of InC_x increased to 4% from 1.5%, observed for the as-grown material. This compound is not observed in the samples irradiated in DI water; instead they exhibit a traceable amount of H_2O. We attribute a reduced concentration of InP_xO_y, observed in the as-grown material exposed to DI water (17%) compared to the 29% concentration of this oxide in the as-grown sample exposed to air, to the high solubility of this oxide in DI water. Following the RTA step at 700 °C for 2 min, the concentration of InP_xO_y, regardless of the pulse number, has been reduced to near 10%. This illustrates the effect of thermal decomposition of oxides and loss of the surface oxygen due to its diffusion into the investigated microstructure. Similar to the results presented in Fig. 7c and d, the surface chemical composition of all the RTA processed samples is indistinguishable within the experimental error of the XPS measurements.

4. Conclusions

We have investigated the surface chemical evolution of InP/InGaAs/InGaAsP QW microstructures irradiated with ArF and KrF lasers in the context of the laser induced QWI effect. The role of laser irradiation, carried out in air and DI water, is to modify the surface of the QW microstructure and create conditions enhancing atomic intermixing during the RTA step. Our results have indicated that InP_xO_y oxides are the dominating product of the ArF and KrF lasers interaction with InP. Owing to oxide solubility in water, a significantly greater concentration of oxides has been observed in samples irradiated in air than in those irradiated in DI water. The increasing oxide concentration with the laser pulse number has a similar trend as the band gap increment, indicating that oxides play important roles in the excimer laser QWI. The SIMS results show that after RTA, significant amount of oxygen atoms have diffused in the microstructure active region and resulted in an enhanced intermixing. A greater PL shift in samples irradiated in air than that in the samples irradiated in DI water is consistent with this observation. XPS results have also shown that surface chemical composition of samples after the RTA step is comparable, regardless of the environment in which the laser irradiation took place. This suggests that excimer laser processing of InP/InGaAs/InGaAsP microstructures

does not lead to a significant modification of the surface chemical composition – a feature attractive for the fabrication of future devices from the laser fabricated QWI material.

Acknowledgements

This work was supported by the Natural Science and Engineering Research Council of Canada (Discovery Grant No. 122795-2010), the programs of the Canada Research Chair in Quantum Semiconductors (JJD), Plasma Québec and CMC Microsystems (Kingston, Ontario). Technical assistance of Sonia Blais (Université de Sherbrooke Centre de characterization de materiaux, Sherbrooke) in collecting XPS data, Suzie Poulin (École Polytechnique Laboratoire de service pour analysis de surface des materiaux, Montréal) in collecting SIMS data and help of the technical staff of the Université de Sherbrooke Centre de recherche en nanofabrication et en nanocaracterisation (CRN^2) is greatly appreciated. NL acknowledges the Merit Scholarship Program for Foreign Student, Fonds de recherche du Québec – Nature et technologies, for providing a graduate student scholarship.

References

[1] H. Lianping, M. Haji, R. Dylewicz, Q. Bocang, A.C. Bryce, 10-GHz mode-locked extended cavity laser integrated with surface-etched DBR fabricated by quantum-well intermixing, IEEE Photonics Technology Letters 23 (2011) 82–84.
[2] A. McKee, C. McLean, G. Lullo, A.C. Bryce, R.M. De La Rue, J.H. Marsh, C.C. Button, Monolithic integration in InGaAs-InGaAsP multiple-quantum-well structures using laser intermixing, IEEE Journal of Quantum Electronics 33 (1997) 45–55.
[3] J. Teng, J. Dong, S. Chua, M. Lai, B. Foo, D. Thompson, B. Robinson, A. Lee, J. Hazell, I. Sproule, Controlled group V intermixing in InGaAsP quantum well structures and its application to the fabrication of two section tunable lasers, Journal of Applied Physics 92 (2002) 4330.
[4] J. Arokiaraj, H.S. Djie, T. Mei, Investigations on the blue-shift phenomena in argon plasma intermixed InGaAs/InGaAsP quantum well structures, Applied Surface Science 237 (2004) 256–260.
[5] Y. Deok Ho, K.H. Yoon, S.J. Kim, Characteristics of intermixed InGaAs/InGaAsP multi-quantum-well structure, Japanese Journal of Applied Physics 39 (2000) 1032–1034.
[6] S.C. Du, L. Fu, H.H. Tan, C. Jagadish, Investigation of ion implantation induced intermixing in InP based quaternary quantum wells, Journal of Physics D 44 (2011) 475105.
[7] J.J. Dubowski, Laser-induced bandgap shifting for photonic device integration. US Patent 6,514,784, 2003.
[8] J. Genest, R. Beal, V. Aimez, J.J. Dubowski, ArF laser-based quantum well intermixing in InGaAs/InGaAsP heterostructures, Applied Physics Letters 93 (2008) 071106.
[9] J. Genest, J.J. Dubowski, V. Aimez, Suppressed intermixing in InAlGaAs/AlGaAs/GaAs and AlGaAs/GaAs quantum well heterostructures irradiated with a KrF excimer laser, Applied Physics A 89 (2007) 423–426.
[10] J. Genest, J.J. Dubowski, V. Aimez, UV laser-based process for quantum well intermixing of III–V heterostructures, Proceeding of SPIE 5451 (2004) 551.
[11] N. Liu, Kh Moumanis, J.J. Dubowski, Self-organized Nano-cone Arrays in InP/InGaAs/InGaAsP Microstructures by Irradiation with ArF and KrF Excimer Lasers, Journal of Laser Micro/Nanoengineering 7 (2012) 130.
[12] N. Liu, S. Blais, J.J. Dubowski, Surface and interface study of SiO coated InP/InGaAs/InGaAsP semiconductor laser microstructures processed in the soft KrF laser irradiation regime, Proceeding of SPIE 8206 (2011) 820609.
[13] N. Liu, Kh. Moumanis, J.J. Dubowski, Surface morphology of SiO2 coated InP/InGaAs/InGaAsP microstructures following irradiation with the ArF and KrF excimer lasers, Proceeding of SPIE 7920 (2011) 79200 C.
[14] C.L. Chiu, E.Y. Lin, K.Y. Chuang, D.J.Y. Feng, T.S. Lay, Argon plasma induced photoluminescence enhancement and quantum well intermixing of InGaAs/InGaAlAs multiple quantum wells, Physica B 404 (2009) 1226–1229.
[15] J.J. Dubowski, P. Poole, G. Sproule, G. Marshall, S. Moisa, C. Lacelle, M. Buchanan, Enhanced quantum-well photoluminescence in InGaAs/InGaAsP heterostructures following excimer-laser-assisted surface processing, Applied Physics A 69 (1999) 299–303.
[16] A. Francois, V. Aimez, J. Beauvais, M. Gendry, P. Regreny, Enhancement of quantum well intermixing on InP/InGaAs/InGaAsP heterostructures using titanium oxide surface stressors to induce forced point defect diffusion, Applied Physics Letters 89 (2006) 164107.
[17] I. McKerracher, L. Fu, H. Tan, C. Jagadish, Impurity-free vacancy disordering of quantum heterostructures with SiO_xN_y encapsulants deposited by magnetron sputtering, Proceedings of SPIE 7039 (2008) 70390U.
[18] N. Holonyak Jr., Impurity-induced layer disordering of quantum-well heterostructures: discovery and prospects, IEEE Journal of Selected Topics in Quantum Electronics 4 (1998) 584–594.
[19] D.G. Deppe, N. Holonyak, Atom diffusion and impurity-induced layer disordering in quantum well III–V semiconductor heterostructures, Journal of Applied Physics 64 (1988) R93–R113.
[20] C.A.A. Ghumman, A.M.C. Moutinho, A. Santos, O.M.N.D. Teodoro, A. Tolstogouzov, An upgraded TOF-SIMS VG Ionex IX23LS: Study on the negative secondary ion emission of IIII–V compound semiconductors with prior neutral cesium deposition, Applied Surface Science 258 (2012) 2490–2497.
[21] L.L. Yang, Q.X. Zhao, G.Z. Xing, D.D. Wang, T. Wu, M. Willander, I. Ivanov, J.H. Yang, A SIMS study on Mg diffusion in $Zn_{0.94}Mg_{0.06}O$/ZnO heterostructures grown by metal organic chemical vapor deposition, Applied Surface Science 257 (2011) 8629–8633.
[22] D. Aspnes, A. Studna, Dielectric functions and optical parameters of Si, Ge, GaP, GaAs, GaSb, InP, InAs, and InSb from 1.5 to 6.0 eV, Physical Review B 27 (1983) 985.
[23] V. Mikushkin, S. Sysoev, Y. Gordeev, Standardless XPS method for determining the chemical composition of multiphase compounds and its application to studies of InP plasma oxide nanofilms, Physics of the Solid State 46 (2004) 1830–1835.
[24] J. Pan, S. Tay, C. Huan, A. Wee, XPS study of incident angle effects on the ion beam modification of InP surfaces by 6 keV O_2, Surface and Interface Analysis 27 (1999) 993–997.
[25] N. Shibata, H. Ikoma, X-ray photoelectron spectroscopic study of oxidation of InP, Japanese Journal of Applied Physics 31 (1992) 3976–3980.
[26] A.M. Salvia, J.E. Castle, The intrinsic asymmetry of photoelectron peaks: dependence on chemical state and role in curve fitting, Journal of Electron Spectroscopy and Related Phenomenon 95 (1998) 45–56.
[27] S. Ingrey, W. Lau, N. McIntyre, R. Sodhi, An X-ray photoelectron spectroscopy study on ozone treated InP surfaces, Journal of Vacuum Science and Technology A5 (1987) 1621–1624.
[28] Y. Feurprier, C. Cardinaud, G. Turban, Surface modification and etch product detection during reactive ion etching of InP in-plasma, Plasma Sources Science and Technology 6 (1997) 334.
[29] Z. Jin, T. Hashizume, H. Hasegawa, In situ X-ray photoelectron spectroscopy study of etch chemistry of methane-based reactive ion beam etching of InP using N_2, Japanese Journal of Applied Physics 40 (2001) 2757.
[30] R. Stanowski, O. Voznyy, J.J. Dubowski, Finite element model calculations of temperature profiles in Nd: YAG laser annealed GaAs/AlGaAs quantum well microstructures, Journal of Laser Micro/Nanoengineering 1 (2006) 17–21.
[31] G. Chen, S. Visbeck, D. Law, R. Hicks, Structure-sensitive oxidation of the indium phosphide (0 0 1) surface, Journal of Applied Physics 91 (2002) 9362.
[32] G. Truesdale, A. Downing, G. Lowden, The solubility of oxygen in pure water and sea-water, Journal of Applied Chemistry 5 (1955) 53–62.
[33] V. Golovanov, M.A. Maki-Jaskari, T.T. Rantala, G. Korotcenkov, V. Brinzari, A. Cornet, J. Morante, Experimental and theoretical studies of indium oxide gas sensors fabricated by spray pyrolysis, Sensors and Actuators B: Chemical 106 (2005) 563–571.
[34] T. Som, T.K. Chini, Y.S. Katharia, S. Tripathy, D. Kanjilal, Formation of nanodots on oblique ion sputtered InP surfaces, Applied Surface Science 256 (2009) 562–566.
[35] G. Hollinger, E. Bergignat, J. Joseph, Y. Robach, On the nature of oxides on InP surfaces, Journal of Vacuum Science & Technology A3 (2009) 2082–2088.
[36] D. Miller, M. Biesinger, N. McIntyre, Interactions of CO_2 and CO at fractional atmosphere pressures with iron and iron oxide surfaces: one possible mechanism for surface contamination? Surface and Interface Analysis 33 (2002) 299–305.
[37] T.P. Nguyen, S. Lefrant, S. De Vos, Y. Gao, Interfacial reactions in poly (phenylene vinylene)-metal systems, Synthetic Metals 84 (1997) 659–660.
[38] A. Baranzahi, A.L. Spetz, I. Lundstrom, Reversible hydrogen annealing of metal-oxide-silicon carbide devices at high temperatures, Applied Physics Letters 67 (1995) 3203.
[39] P. Schulze, S. Shaffer, R. Hance, D. Utley, Adsorption of water on rhenium studied by XPS, Journal of Vacuum Science and Technology 1 (1983) 97–99.
[40] J.C.C. Fan, J.B. Goodenough, X-ray photoemission spectroscopy studies of Sn-doped indium-oxide films, Journal of Applied Physics 48 (1977) 3524–3531.
[41] M. Yamaguchi, K. Ando, Thermal oxidation of InP and properties of oxide film, Journal of Applied Physics 51 (1980) 5007–5012.
[42] W. Lau, R. Sodhi, S. Ingrey, Thermal desorption of oxides on InP, Applied Physics Letters 52 (1988) 386–388.
[43] C. Abernathy, S. Pearton, R. Caruso, F. Ren, J. Kovalchik, Ultrahigh doping of GaAs by carbon during metalorganic molecular beam epitaxy, Applied Physics Letters 55 (1989) 1750–1752.
[44] O. Gunawan, T. Ong, Y. Chen, B. Ooi, Y. Lam, Y. Zhou, Y. Chan, A theoretical analysis of quantum well intermixing using the pulsed laser irradiation technique in InGaAs/InGaAsP laser structure, Surface and Coatings Technology 130 (2000) 116–121.
[45] T. Kitatani, M. Kondow, T. Tanaka, Effects of thermal annealing procedure and a strained intermediate layer on a highly-strained GaInNAs/GaAs double-quantum-well structure, Journal of Crystal Growth 221 (2000) 491–495.
[46] T. Tsuchiya, J. Shimizu, M. Shirai, M. Aoki, Selective-area growth of high-crystalline-quality InGaAlAs by metal-organic vapor-phase epitaxy, Journal of Crystal Growth 248 (2003) 384–389.
[47] L. Guido, J. Major, J. Baker, N. Holonyak, R. Burnham, Disorder defined buried heterostructure $Al_xGa_{1-x}As$/GaAs quantum well lasers by diffusion of silicon and oxygen from Al-reduced SiO_2, Applied Physics Letters 54 (1989) 1265–1267.